Timing Recovery Based on the PAM Representation of CPM

Erik Perrins and Sayak Bose
Department of Electrical Engineering & Computer Science
University of Kansas, Lawrence, KS 66045
E-mail: esp@ieee.org, sayak@ku.edu

Marilynn P. Wylie-Green
Nokia Siemens Networks
Irving, Texas 75063
E-mail: marilynn.green@nsn.com

***Abstract*— A reduced-complexity decision-directed timing recovery method for continuous phase modulation (CPM) is presented. Using the well-known and popular pulse amplitude modulation (PAM) representation—or Laurent representation—of CPM, we develop two different formulations of a PAM-based timing error detector (TED). We consider the general *M*-ary multi-*h* CPM model in our development and use the family of aeronautical telemetry CPMs for our numerical examples. We show by analysis that the two TED formulations have identical "S-curve" characteristics, and are free of false lock points, but have slightly different performance when applied to specific CPM examples, particularly in the multi-*h* case. There is no unanimous winner between the two formulations in all cases; however, for both formulations, we show the TEDs are able to perform close to the theoretical limit given by the modified Cramer-Rao bound. As such, the proposed TEDs provide an important synchronization component for reduced-complexity PAM-based CPM receivers that has heretofore been missing.**

I. Introduction

Continuous phase modulation (CPM) [1] is a jointly power and bandwidth efficient digital modulation scheme used for data transmission over bandlimited non-linear channels. Its constant-envelope nature allows simple (inexpensive) transmitters and high efficiency in converting source power into radiated power, which is critical in mobile (i.e. battery powered) applications. The transmitter-friendliness of CPM makes it a natural choice in applications where simple analog components and/or mobile power efficiency are desired on the transmit side. However, its deployment beyond the family of minimum-shift keying (MSK)-type versions has been limited in large part because of its nonlinear nature and the complexity and synchronization problems that arise therefrom.

One popular method of dealing with the challenges of CPM has been the pulse amplitude modulation (PAM) representation. This is a method of "linearizing" CPM that was first proposed for binary CPMs in the well-known paper by Laurent [2]. This method has since been extended to M-ary CPM [3], multi-h CPM [4], and cases such as integer modulation index [5] and data-dependent pulses [6], among others. It has been applied to the design of reduced-complexity detectors [7]–[9], carrier phase recovery [8] and carrier frequency recovery [10].

In this paper, we apply the PAM representation of CPM to the problem of symbol timing recovery for CPMs in general. The problem of timing recovery for CPM has received regular attention over the years. In [11], a non-data-aided timing recovery scheme was developed, and in [12] a decision-directed joint phase and timing recovery scheme was developed using a conventional (i.e. non-PAM) CPM representation. In [13] a joint time and phase synchronization scheme was proposed based on nonorthogonal exponential expansions and Kalman filtering. None of these previous studies were based on the reduced-complexity PAM representation of CPM. In [14], the PAM representation was applied to timing recovery for the special case of MSK-type signals, but not for CPM in general.

The proposed decision-directed PAM-based timing recovery scheme is valid for CPMs in general and complements the previous work that has been done for reduced-complexity PAM-based detection and synchronization for CPM, i.e. [7]–[10]. As such, the proposed scheme provides an important synchronization component for PAM-based CPM receivers that has been missing up to this point. We exploit the decision-directed nature of the algorithm to develop two formulations of the reduced-complexity PAM-based timing error detector (TED) that have different arrangements of the front-end matched filters (MFs). We show that both TED formulations have identical reduced-complexity filtering requirements and identical "S-curve" characteristics and both are free of false-lock points. We use the family of three aeronautical telemetry CPMs [15] as case studies for the proposed approach. There is no unanimous winner between the two TED formulations in all cases; however, we give numerical results for normalized timing error variance that show that both TED formulations are able to perform close to the modified Cramer-Rao bound (MCRB). Therefore, it is recommended that both formulations be considered in the receiver design process for a given CPM scheme.

II. Signal Model

A. Conventional CPM model

We consider the CPM signal with complex envelope [1]

$$s(t;\boldsymbol{\alpha}) \triangleq \sqrt{\frac{E_s}{T_s}} \exp\{j\phi(t;\boldsymbol{\alpha})\} \tag{1}$$

This work was supported in part by Nokia Siemens Networks through the Information & Telecommunications Technology Center at the University of Kansas.

where E_s is the symbol energy and T_s is the symbol duration. The phase of the signal is given by

$$\phi(t;\boldsymbol{\alpha}) \triangleq 2\pi \sum_i \alpha_i h_{\underline{i}} q(t - iT_s) \tag{2}$$

where $\boldsymbol{\alpha} \triangleq \{\alpha_i\}$ is a sequence of M-ary data symbols and $\{h_i\}_{i=0}^{N_h-1}$ is a set of N_h *modulation indexes*.[1] The *phase response* $q(t)$ is defined as the time-integral of the *frequency pulse* $f(t)$, which has a duration of L symbol times and an area of 1/2. When $L = 1$ the signal is said to be *full-response* and when $L > 1$ the signal is said to be *partial-response*. Some common pulse shapes are length-LT_s rectangular (LREC), length-LT_s raised-cosine (LRC), and Gaussian, which are all defined in [16, p. 119].

The phase $\phi(t;\boldsymbol{\alpha})$ in (2) can be expressed as

$$\phi(t;\boldsymbol{\alpha}) = \eta(t;\mathbf{c}_n) + \theta_{n-L}, \qquad nT_s \le t < (n+1)T_s, \tag{3}$$

where

$$\eta(t;\mathbf{c}_n) \triangleq 2\pi \sum_{i=n-L+1}^{n} \alpha_i h_{\underline{i}} q(t - iT_s),$$

$$\mathbf{c}_n \triangleq [\alpha_{n-L+1}, \cdots, \alpha_{n-1}, \alpha_n], \tag{4}$$

and

$$\theta_{n-L} \triangleq \pi \sum_{i=0}^{n-L} \alpha_i h_{\underline{i}} \bmod 2\pi. \tag{5}$$

In the above equations, $\mathbf{c}_n$ is the *correlative state vector*, θ_{n-L} is the *phase state*, and n is the *current symbol index*.

For the important special case where the modulation indexes are rational numbers, i.e. $h_i = k_i/p$, $0 \le i \le N_h - 1$, the phase states are drawn from a *finite* alphabet of $2p$ points evenly distributed around the unit circle. Using the *tilted phase* representation in [17], the phase state alphabet can be cut in half, i.e. a set of p points evenly distributed around the unit circle. Therefore, the signal in (3) can be represented by a phase trellis of $N_S = pM^{L-1}$ states, where each branch is associated with a unique value of the *branch vector* $[\theta_{n-L}, \mathbf{c}_n]$.

B. PAM-based CPM model

In the well-known paper by Laurent [2], it was shown that the right-hand side of (1) can be formulated as a superposition of data-modulated pulses for the special case of binary ($M = 2$) single-h CPM with non-integer modulation index. This pulse amplitude modulation (PAM) representation of CPM has since been extended to M-ary CPM [3], multi-h CPM [4], and cases such as integer modulation index [5] and data-dependent pulses [6], among others. In order to expedite our development, we restrict ourselves to the cases considered in [2]–[4] and note that the proposed PAM-based timing recovery methods can be extended to other cases.

Using the PAM-based model for M-ary multi-h CPM, the right-hand side of (1) can be *exactly* represented as [4]

$$s(t;\boldsymbol{\alpha}) = \sqrt{\frac{E_s}{T_s}} \sum_{k=0}^{N-1} \sum_i b_{k,i} g_{k,\underline{i}}(t - iT_s) \tag{6}$$

[1] In this paper, the underlined subscript notation in (2) is defined as modulo-N_h, i.e. $\underline{i} \triangleq i \bmod N_h$. When $N_h = 1$ we have *single-h* CPM, which is the most common case. When $N_h \ge 1$ we have the less-common *multi-h* CPM case.

where the number of PAM components is $N = 2^{P(L-1)}(M-1)$ and $P = \log_2(M)$ when the alphabet size M is an integer power of 2. The pseudo-symbols $\{b_{k,i}\}_{k=0}^{N-1}$ have a lengthy definition that is not summarized here but is instead found in [4] for the general multi-h case, with special cases found in [2], [3]; suffice it to say that the pseudo-symbols are a non-linear function of the symbol sequence $\boldsymbol{\alpha}$. Likewise, the PAM signal pulses $\{g_{k,\underline{i}}(t)\}_{k=0}^{N-1}$, which vary greatly in amplitude and duration, are defined in [2]–[4] for the respective cases; the k-th pulse has a duration of D_k symbol times, where D_k is an integer in the range $1 \le D_k \le L+1$.

Based on the definition of the pseudo-symbols, the phase state θ_{i-L} can be factored out of $b_{k,i}$, leaving a term that is a function of the correlative state vector $\mathbf{c}_i$, i.e.

$$s(t;\boldsymbol{\alpha}) = \sqrt{\frac{E_s}{T_s}} \sum_i e^{j\theta_{i-L}} \sum_{k=0}^{N-1} b_k(\mathbf{c}_i) g_{k,\underline{i}}(t - iT_s). \tag{7}$$

An important aspect of (7) which we summarize and emphasize here is the *PAM complexity reduction principle*, which has been used to formulate reduced-complexity detectors [7]. The first step is to exploit the fact that the pulses with the largest amplitudes also have the longest durations (i.e. the most energy), and that there are only a few such pulses [2], [3]. The indexes of these pulses are grouped in the subset $\mathcal{K}$, where $\mathcal{K} \subseteq \{0, 1, \cdots, N-1\}$ and has $|\mathcal{K}|$ elements. ($A \subseteq B$ denotes that A is a subset of B.) The reduced number of pulses has the net effect of reducing the number of MFs in the detector [7].

The second complexity-reduction step is to observe that with the pseudo-symbols that remain, i.e. $\{b_k(\mathbf{c}_i)\}_{k\in\mathcal{K}}$, it is possible to factor out additional data symbols, starting with α_{i-L+1}, which has the net effect of *shortening* the correlative state vector and thereby reducing the number of trellis states in the detector [7]. The full correlative state vector $\mathbf{c}_n$ in (4) contains L elements, whereas the shortened correlative state vector $\mathbf{c}'_n$ contains only $L' \le L$ elements; the elements that are removed from $\mathbf{c}'_n$, namely $\{\alpha_i\}_{i=n-L+1}^{n-L'}$, are *absorbed* into the phase state $\theta_{n-L'}$. The value of L' is determined by the choice of $\mathcal{K}$, and although the inner-workings of this relationship are intricate, it was shown in [9] that the duration of the *shortest PAM pulse* is a readily-available means of identifying L', via the relation

$$L' = \begin{cases} L - D_{\min} + 1, & D_{\min} < L+1 \\ 1, & D_{\min} = L+1 \end{cases}, \text{ where } D_{\min} \triangleq \min_{k\in\mathcal{K}} D_k.$$

The concepts outlined above are used to formulate reduced-complexity PAM-based detectors.

III. PAM-Based Timing Error Detector

We derive the PAM-based timing error detector (TED) using maximum likelihood principles. The signal observed at the receiver is modeled as

$$r(t) = s(t - \tau;\boldsymbol{\alpha}) + w(t) \tag{8}$$

where $w(t)$ is complex-valued additive white Gaussian noise (AWGN) with zero mean and power spectral density N_0. The variables $\boldsymbol{\alpha}$ and τ represent the data symbols and the symbol

timing, respectively. In practice, both of these variables are unknown to the receiver and both must be recovered.

In what follows, we refer to estimated and hypothesized values of a generic quantity x as $\hat{x}$ and $\tilde{x}$, respectively. Also, $\hat{x}$ and $\tilde{x}$ can assume the same values as x itself.

A. Maximum likelihood PAM-based sequence detection

The symbol sequence $\boldsymbol{\alpha}$ can be recovered using maximum likelihood sequence detection (MLSD). In [1], it was shown that the log-likelihood function for the hypothesized symbol sequence $\tilde{\boldsymbol{\alpha}}$ over the observation interval $0 \le t \le L_0 T_s$ is

$$\Lambda(\boldsymbol{r}|\tilde{\boldsymbol{\alpha}}) = \mathrm{Re}\left\{ \int_0^{L_0 T_s} r(t) s^*(t-\tau;\tilde{\boldsymbol{\alpha}})\, dt \right\} \tag{9}$$

where we assume for the moment that τ is known and $(\cdot)^*$ denotes the complex conjugate. Applying $\mathcal{K}$ to (7) and inserting the resulting expression into (9) yields

$$\Lambda(\boldsymbol{r}|\tilde{\boldsymbol{\alpha}}) \approx \mathrm{Re}\left\{ \int_0^{L_0 T_s} r(t) \sum_i e^{-j\tilde{\theta}_{i-L'}} \sum_{k\in\mathcal{K}} b_k^*(\tilde{\mathbf{c}}_i') g_{k,\underline{i}}(t-\tau-iT_s) dt \right\}.$$

Changing the order of integration and summation results in

$$\Lambda(\boldsymbol{r}|\tilde{\boldsymbol{\alpha}}) \approx \sum_{i=0}^{L_0-1} \mathrm{Re}\big\{ y_i(\tilde{\mathbf{c}}_i', \tilde{\theta}_{i-L'}, \tau) \big\} \tag{10}$$

which is a function that can be maximized efficiently using the Viterbi algorithm (VA), e.g. [1, Ch. 7]. The *metric increment* $y_i(\tilde{\mathbf{c}}_i', \tilde{\theta}_{i-L'}, \tau)$ is defined as [9]

$$y_i(\tilde{\mathbf{c}}_i', \tilde{\theta}_{i-L'}, \tau) \triangleq e^{-j\tilde{\theta}_{i-L'}} \sum_{k\in\mathcal{K}} b_k^*(\tilde{\mathbf{c}}_i') x_{k,i}(\tau). \tag{11}$$

The time-reversed PAM pulses $\{g_{k,\underline{i}}(-t)\}_{k\in\mathcal{K}}$ serve as the impulse responses of the MF bank [7], [9], with outputs defined as

$$x_{k,i}(\tau) \triangleq \int_{\tau+iT_s}^{\tau+(i+D_k)T_s} r(t) g_{k,\underline{i}}(t-\tau-iT_s)\, dt \tag{12}$$

where the sampling instant varies with the pulse duration D_k. The implementation of the MF bank requires a delay of LT_s in order to make the longest impulse response causal.

At this point, we summarize key attributes of (11) and (12): 1) the interval of integration in (12) is formulated to span *multiple* symbol intervals, and 2) for the current time step n within the VA, the metric increment $y_n(\tilde{\mathbf{c}}_n', \tilde{\theta}_{n-L'}, \tau)$ is a function only of the current *shortened* branch vector $[\tilde{\theta}_{n-L'}, \tilde{\mathbf{c}}_n']$ and therefore requires a trellis of only $pM^{L'-1}$ states. The steps taken in the derivation of (11) and (12) were motivated by state complexity reduction, which is not necessarily a concern in the timing recovery problem.

B. Maximum likelihood PAM-based timing recovery

In order to recover τ, we temporarily assume that $\boldsymbol{\alpha}$ is known. Using the above definitions, it can be shown that the likelihood function for a hypothesized timing value $\tilde{\tau}$ is

$$\Lambda(\boldsymbol{r}|\tilde{\tau}) = \mathrm{Re}\left\{ \int_0^{L_0 T_s} r(t) s^*(t-\tilde{\tau};\boldsymbol{\alpha})\, dt \right\}. \tag{13}$$

The maximum of $\Lambda(\boldsymbol{r}|\tilde{\tau})$ with respect to $\tilde{\tau}$ is obtained by setting equal to zero the partial derivative of (13) with respect to $\tilde{\tau}$. Thus, we obtain

$$\mathrm{Re}\left\{ -\int_0^{L_0 T_s} r(t) \dot{s}^*(t-\tilde{\tau};\boldsymbol{\alpha})\, dt \right\} = 0 \tag{14}$$

where $\dot{s}(t)$ is the time-derivative of $s(t)$.

In formulating the solution to (14), we make the salient observation that detecting $\boldsymbol{\alpha}$ and estimating τ are *separate problems* and do not necessarily require 1) the same effort to reduce state complexity since $\boldsymbol{\alpha}$ is assumed to be known, and 2) the same subset of PAM components in order to achieve satisfactory performance. With respect to the latter issue, we allow the TED to be based on a possibly different subset of PAM components, $\mathcal{K}_{\text{TED}}$, where $\mathcal{K}_{\text{TED}} \subseteq \mathcal{K} \subseteq \{0, 1, \cdots, N-1\}$. This possibly reduces the number filters needed to support the TED, because *filter complexity* is still a concern even though *state complexity* is not. With respect to the relaxation of the state complexity issue, we have the freedom to develop two slightly different formulations of the PAM-based TED.

The first TED formulation parallels (10)–(12) which yields

$$\sum_{i=0}^{L_0-1} \mathrm{Re}\left\{ \dot{y}_i(\mathbf{c}_i, \theta_{i-L}, \tilde{\tau}) \right\} = 0 \tag{15}$$

where the TED increment $\dot{y}_i(\mathbf{c}_i, \theta_{i-L}, \tilde{\tau})$ is given by[2]

$$\dot{y}_i(\mathbf{c}_i, \theta_{i-L}, \tilde{\tau}) = \sum_{k\in\mathcal{K}_{\text{TED}}} b_{k,i}^* \dot{x}_{k,i}(\tilde{\tau}) \tag{16}$$

and $\dot{x}_{k,i}(t)$ is the time derivative of $x_{k,i}(t)$. A discrete-time differentiator is used to implement $\dot{x}_{k,i}(t)$, as discussed momentarily.

We begin the formulation of the second TED by breaking the interval of integration in (14) into non-overlapping length-T_s segments, i.e.

$$\mathrm{Re}\left\{ -\sum_{i=0}^{L_0-1} \int_{iT_s}^{(i+1)T_s} r(t) \dot{s}^*(t-\tilde{\tau};\boldsymbol{\alpha})\, dt \right\} = 0. \tag{17}$$

Then, inserting (6) into (17) and rearranging terms yields

$$\sum_{i=0}^{L_0-1} \mathrm{Re}\left\{ \dot{z}_i(\mathbf{c}_i, \theta_{i-L}, \tilde{\tau}) \right\} = 0 \tag{18}$$

where the TED increment $\dot{z}_i(\mathbf{c}_i, \theta_{i-L}, \tilde{\tau})$ is

$$\dot{z}_i(\mathbf{c}_i, \theta_{i-L}, \tilde{\tau}) = \sum_{k\in\mathcal{K}_{\text{TED}}} \sum_{l=i-D_k+1}^{i} b_{k,l}^* \dot{x}_{k,i,l}(\tilde{\tau}) \tag{19}$$

and $\dot{x}_{k,i,l}(\tau)$ is the derivative with respect to τ of

$$x_{k,i,l}(\tau) \triangleq \int_{\tau+iT_s}^{\tau+(i+1)T_s} r(t) g_{k,\underline{l}}(t-\tau-lT_s)\, dt. \tag{20}$$

[2]This TED increment could be formulated just as easily with the shortened value L', i.e. $\dot{y}_i(\mathbf{c}_i', \theta_{i-L'}, \tilde{\tau})$; however, for the sake of consistent notation between the two TEDs we do not use L'.

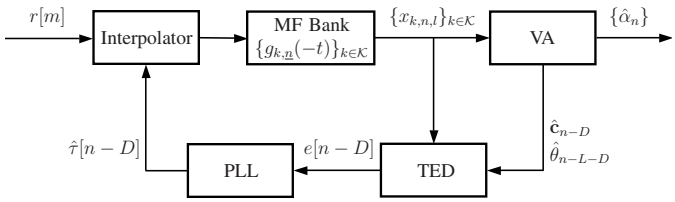

Fig. 1. Discrete-time implementation of the PAM-based decision-directed timing recovery system for multi-h CPM.

C. TED implementation

Conceptually speaking, the key attributes of the increment in (16) are that the pseudo-symbols are fixed by the index i and the interval of integration spans multiple symbol times. On the other hand, with the increment in (19) the single-symbol interval of integration is fixed by the index i and the pseudo-symbols span multiple symbol times. Both implementations require the exact same *amount* of filtering (i.e. integration) and differ only in the manner in which the filter outputs are sampled and combined. In fact, it should be noted that the length-D_kT_s filter outputs $x_{k,i}(\tau)$ can be obtained by proper combination of the length-T_s filter outputs $x_{k,i,l}(\tau)$, and thus only one filter bank is required for the receiver.

The solutions to (15) and (18) [i.e. the value of $\tilde{\tau}$ that causes the left-hand side of the equations to vanish] is obtained in an adaptive/iterative manner. As they are formulated, (15) and (18) assume the true data sequence $\{\cdots, \alpha_{n-2}, \alpha_{n-1}, \alpha_n\}$ is known, which is not the case in practice. A logical substitute for the true data sequence is the sequence of tentative decisions within the VA, which become more reliable the further we trace back along the trellis. Considering all these factors, we formulate the following PAM-based timing error signals

$$e[n-D] = \mathrm{Re}\left\{\dot{y}_{n-D}(\hat{\mathbf{c}}_{n-D}, \hat{\theta}_{n-L-D}, \hat{\tau}[n-D])\right\} \quad (21a)$$

or

$$e[n-D] = \mathrm{Re}\left\{\dot{z}_{n-D}(\hat{\mathbf{c}}_{n-D}, \hat{\theta}_{n-L-D}, \hat{\tau}[n-D])\right\} \quad (21b)$$

where D is the traceback depth (delay) for computing the error and $\hat{\mathbf{c}}_{n-D}$ and $\hat{\theta}_{n-L-D}$ are taken from the path history of the best survivor in the VA. The PAM-based timing error signals in (21) have features in common with the one derived in [12] using the conventional CPM model in (1). A large D could result in longer delays in the timing recovery loop, but our observation in Section V, which parallels the finding in [12], is that $D = 1$ produces satisfactory results. From this point on, we refer to (21a) as "TED-A" and (21b) as "TED-B."

Fig. 1 shows a discrete-time implementation of the sequence detection operation in (10) and either TED operation in (21). The discrete-time received signal $r[m]$ is sampled at a rate of N samples per symbol. A sample interpolator is used to synchronize the received signal based on the most recent timing estimate, $\hat{\tau}[n-D]$. The synchronized samples are fed to the MF bank, the outputs of which form the values in the set $\{x_{k,n,l}\}_{k\in\mathcal{K}}$. The MF outputs are sampled at the symbol rate at the proper timing instant, and these MF samples are used to update the branch metrics within the VA, i.e. (10). In addition to the samples of $\{x_{k,n,l}\}_{k\in\mathcal{K}}$ that are used in the VA, an *early* sample of each $\{x_{k,n,l}\}_{k\in\mathcal{K}_{\text{TED}}}$ is taken, as well as a *late* sample. The *difference* between the early and late samples is used to approximate the *derivative* $\dot{x}_{k,n,l}(t)$. This procedure is detailed further in [12]. Once the error signal $e[n-D]$ is formed, it is fed to a phase-locked loop (PLL),[3] which in turn outputs the timing estimate $\hat{\tau}[n-D]$.

IV. Performance Analysis

A. Modified Cramer-Rao bound for multi-h CPM

We use the modified Cramer-Rao bound (MCRB) [18] to establish a lower bound on the degree of accuracy to which τ can be estimated. The formulas given in [11], [19] require slight modification to be applicable to multi-h CPM. Following the approach in [19, Ch. 2] the complete complex-baseband signal model is represented as

$$s(t;\boldsymbol{\alpha},\tau) = \sqrt{\frac{E_s}{T_s}}\exp\left\{j\phi(t-\tau;\boldsymbol{\alpha})\right\}. \quad (22)$$

The MCRB with respect to τ for a baseband signal is defined as [19]

$$\mathrm{MCRB}(\tau) \triangleq \frac{N_0/2}{\mathrm{E}_{\boldsymbol{\alpha}}\left\{\int_0^{T_0}\left|\frac{\partial s(t;\boldsymbol{\alpha},\tau)}{\partial\tau}\right|^2 dt\right\}}$$

where $T_0 \triangleq L_0T_s$ is the length of the observation interval and we assume that L_0 is an integer multiple of N_h. Using the signal model in (22), and after taking the partial derivative with respect to τ, we find that we must evaluate the integral

$$T_s\int_0^{T_0}\sum_i h_{\underline{i}}^2 f^2(t-\tau-iT_s).$$

The integration and summation can be arranged in such a way that the easy-to-compute terms

$$C_f \triangleq T_s\int_0^{LT_s} f^2(t)\,dt \quad (23)$$

and

$$\overline{h^2} \triangleq \frac{1}{N_h}\sum_{i=0}^{N_h-1} h_i^2 \quad (24)$$

can be separated from each other. The *mean-squared modulation index* $\overline{h^2}$ in (24) is the modification needed to accommodate multi-h CPM.

The final expression for the MCRB (normalized to the symbol rate) is

$$\frac{1}{T_s^2}\times\mathrm{MCRB}(\tau) = \frac{1}{8\pi^2\overline{h^2}C_\alpha C_f L_0}\times\frac{1}{E_s/N_0} \quad (25)$$

where $C_\alpha \triangleq \mathrm{E}\{\alpha_n^2\} = (M^2-1)/3$ for uncorrelated M-ary data symbols. For the special case of LREC we have $C_f = C_{L\text{REC}} \triangleq 1/(4L)$, and for the special case of LRC we have $C_f = C_{L\text{RC}} \triangleq 3/(8L)$. For all other frequency pulse shapes, (23) can be computed analytically or numerically.

In Section V, we use the MCRB to evaluate computer simulation results for the *normalized timing error variance*, which is defined as

$$\frac{1}{T_s^2}\times\sigma_\tau^2 \triangleq \frac{1}{T_s^2}\times\mathrm{Var}\left\{\hat{\tau}[n]-\tau\right\}. \quad (26)$$

[3]We have shown the TED in a feedback/PLL configuration; however, the TED can just as easily be used in a feedforward configuration.

B. PLL considerations

The final MCRB expression in (25) is formulated in terms of L_0. We use the conversion $L_0 = \frac{1}{2BT_s}$ to relate the *normalized loop bandwidth* BT_s of a feedback-based scheme to the observation length L_0 of a feedforward-based scheme; this relationship is valid for a first-order PLL [12]. Using a standard first-order PLL implementation, the raw TED output $e[n]$ is refined into a more stable timing estimate $\hat{\tau}[n]$ via the update $\hat{\tau}[n] \triangleq \hat{\tau}[n-1] + \gamma e[n]$ which is performed after each symbol time. The PLL *step size* is $\gamma \triangleq \frac{4BT_s}{k_p}$ where the constant k_p is obtained from the so-called *S-curve* characteristic of the TED.

C. S-Curve of the TED

The S-curve is a useful tool for characterizing the behavior of the TED; it is defined as the *expected value* of the TED output $e[n]$ as a function of the *timing offset*, i.e.

$$S(\delta) \triangleq \sqrt{E_s/T_s} \cdot \mathrm{E}\big\{e[n] \,|\, \delta\big\}, \tag{27}$$

where the timing offset is defined as $\delta \triangleq \tau - \hat{\tau}$. The S-curve gives an easy method of identifying the stable lock points for the TED (these are the zero-crossing points on the curve where the slope is positive) and thus determining whether any false-lock points exist. The S-curve also determines the value of k_p, which is the slope of the S-curve evaluated at $\delta = 0$.

The expectation in (27) is taken over the data symbols $\boldsymbol{\alpha}$, the alignment of the modulation indexes $\{h_i\}_{i=0}^{N_h-1}$, and the additive noise. It may come as a surprise that an analytical derivation of the S-curves for TED-A and -B yields identical results. While this equivalence is important to note, we present these final S-curve expressions with distinct formulations in order to accentuate subtle differences between the two TEDs later in Section V. We now give a detailed derivation of the S-curve for TED-A under the assumption that we have perfect knowledge of the transmitted symbol sequence $\boldsymbol{\alpha}$ (i.e. the *data-aided* case). In the case of TED-B, we state only the final result due to lack of space.

We start by making use of the fact that only the difference between τ and $\hat{\tau}$ is important; therefore, we use the substitution $\delta = \tau - \hat{\tau}$ to replace τ and set $\hat{\tau} = 0$ for convenience. Inserting (21a), (16), and the derivative of (12) into (27) yields

$$S(\delta) = -\sqrt{\frac{E_s}{T_s}}\mathrm{E}\left\{\mathrm{Re}\left\{\sum_{k\in\mathcal{K}_{\text{TED}}} b_{k,n}^* \int_{nT_s}^{(n+D_k)T_s} r(t)\dot{g}_{k,\underline{n}}(t-nT_s)dt\right\}\middle|\,\delta\right\}.$$

We next insert (8), with $s(t;\boldsymbol{\alpha})$ given by (6), into the above expression which, after exploiting the fact that the noise has zero mean and is independent of the information symbols, yields the final expression

$$S(\delta) = -\frac{E_s}{T_s}\frac{1}{N_h}\sum_{n=\langle N_h\rangle}\sum_{k\in\mathcal{K}_{\text{TED}}}\int_{nT_s}^{(n+D_k)T_s}\sum_{q=0}^{N-1}\sum_{i=I_1}^{I_2} A_{q,k}(\underline{i}, n-i)g_{q,\underline{i}}(t-\delta-iT_s)\dot{g}_{k,\underline{n}}(t-nT_s)\,dt \tag{28}$$

where

$$A_{q,k}(\underline{i}, n-i) \triangleq \mathrm{E}\left\{b_{q,i}b_{k,n}^*\right\}$$

is the cross-correlation function of the pseudo-symbols, which is real-valued and is given in closed-form in [4].[4] The limits for the summation on i are

$$I_1 = \left\lfloor \frac{t-\delta}{T_s} \right\rfloor - D_q + 1 \text{ and } I_2 = \left\lfloor \frac{t-\delta}{T_s} \right\rfloor$$

with $\lfloor\cdot\rfloor$ denoting the *floor* function, i.e. the largest integer less than or equal to the argument. The outermost summation in (28) has the limits $n = \langle N_h\rangle$, which indicates a range of N_h successive integers that begins with any value of n. In fact, we may view the S-curve in (28) as the average of N_h *component* S-curves, one for each alignment of the modulation indexes.

The final expression for the S-curve for TED-B is

$$S(\delta) = -\frac{E_s}{T_s}\frac{1}{N_h}\sum_{n=\langle N_h\rangle}\sum_{k\in\mathcal{K}_{\text{TED}}}\sum_{i=n-D_k+1}^{n}\int_{nT_s}^{(n+1)T_s}\sum_{q=0}^{N-1}\sum_{l=L_1}^{L_2} A_{q,k}(\underline{l}, i-l)g_{q,\underline{l}}(t-\delta-lT_s)\dot{g}_{k,\underline{i}}(t-iT_s)\,dt \tag{29}$$

where the limits for the summation on l are $L_1 = I_1$ and $L_2 = I_2$. As mentioned earlier, it can be shown that (28) and (29) are equivalent; however, it is interesting to note that the N_h component S-curves that make up the final S-curve are in fact different for TED-A and -B; this difference is explored further in Section V.

We obtain k_p as $k_p \triangleq dS(\delta)/d\delta|_{\delta=0}$, which yields

$$k_p = \frac{E_s}{T_s}\frac{1}{N_h}\sum_{n=\langle N_h\rangle}\sum_{k\in\mathcal{K}_{\text{TED}}}\int_{nT_s}^{(n+D_k)T_s}\sum_{q=0}^{N-1}\sum_{i=I_1}^{I_2} A_{q,k}(\underline{i}, n-i)\dot{g}_{q,\underline{i}}(t-iT_s)\dot{g}_{k,\underline{n}}(t-nT_s)\,dt \tag{30}$$

for TED-A and

$$k_p = \frac{E_s}{T_s}\frac{1}{N_h}\sum_{n=\langle N_h\rangle}\sum_{k\in\mathcal{K}_{\text{TED}}}\sum_{i=n-D_k+1}^{n}\int_{nT_s}^{(n+1)T_s}\sum_{q=0}^{N-1}\sum_{l=L_1}^{L_2} A_{q,k}(\underline{l}, i-l)\dot{g}_{q,\underline{l}}(t-lT_s)\dot{g}_{k,\underline{i}}(t-iT_s)\,dt \tag{31}$$

for TED-B. Here again, the N_h component k_p values that make up the final k_p values are in fact different for TED-A and -B but yield the same *average* value.

V. Numerical Results

A. ARTM CPM: $M = 4$, 3RC, $h = \{4/16, 5/16\}$

We first discuss the S-curves obtained for the multi-h CPM scheme with $M = 4$, 3RC, and $h = \{4/16, 5/16\}$, which is known as "ARTM CPM" (advanced range telemetry CPM) in the IRIG 106-04 aeronautical telemetry standard [15]. The optimal PAM-based detector for this scheme requires a 256-state trellis and a bank of 48×2 multi-h MFs/pulses. There are numerous reduced-complexity PAM-based detector configurations that could be chosen, cf. [20]; of these, we select the 64-state detector with $L' = 2$ that uses a bank of $|\mathcal{K}| = |\mathcal{K}_{\text{TED}}| = 3 \times 1$ MFs/pulses that have been averaged into the equivalent of single-h MFs/pulses, which is suboptimal by only 0.19 dB in terms of detection efficiency [20, Table IV]. In this example, and in all others in this section, we select the TED tentative decision delay as $D = 1$.

[4] It is worth mentioning that for the single-h case the notation for the autocorrelation simplifies to $A_{q,k}(n-i)$ [3].

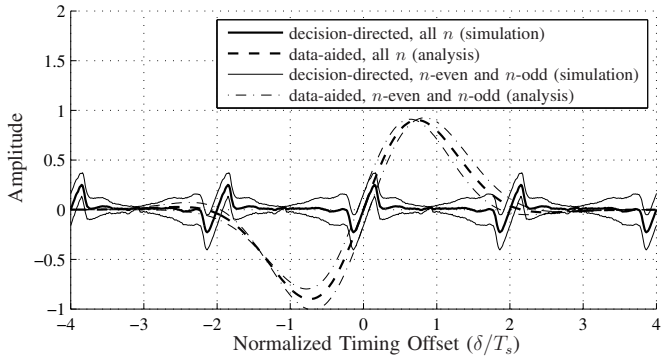

(a)

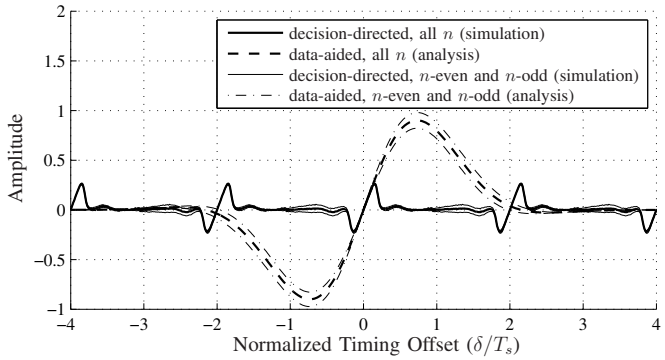

(b)

Fig. 2. S-curves for (a) ARTM CPM with TED-A, and (b) ARTM CPM with TED-B. In each case, the data-aided (analytical) curve is computed for $|\mathcal{K}_{\text{TED}}| = 3 \times 1$. Also, in each case the curve is also computed via simulation for the decision-directed case.

Fig. 2 (a) shows analytical (data-aided) S-curves for TED-A for this detector obtained from numerical computations of (28), which are shown as dashed curves in the figure. We have shown the final S-curve (heavier line weight) as well as the component S-curves for n-even and n-odd (lighter line weights). The curves indicate that TED-A locks onto the correct timing instant at $\delta = 0$ when averaged over all modulation index alignments, but shows a slight forward (or backward) bias for n-even (or n-odd). This analytically-predicted behavior is confirmed with computer simulations for the *decision-directed* case, which is the intended implementation of the TED in practice; the decision-directed curves are shown as solid curves in the figure. We note that the decision-directed S-curves are periodic with period $N_h T_s$, and therefore have stable lock points when δ equals an integer multiple of $N_h T_s$. The simulated S-curves show strong agreement with the analytical S-curves for small values of $|\delta|$, but the performance of the decision-directed TED breaks down as δ approaches half-integer multiples of T_s due to unreliable tentative decisions within the VA. The simulated values of k_p also show strong agreement with (30) and (31).

The presence of an alternating timing bias—with zero bias on average—raises the question of whether or not this should be taken into account during the operation of the algorithm. To answer this question, we compare the normalized timing error variance (26) of TED-A with and without taking the bias into account[5]; these results are shown in Fig. 3 for $BT_s = 1 \times 10^{-3}$ along with the theoretical lower bound given by the MCRB. The results in the figure indicate that better tracking accuracy is achieved by *not* taking the bias into account. Simulations for other multi-h CPM schemes yield the same result but are not shown here due to space constraints.

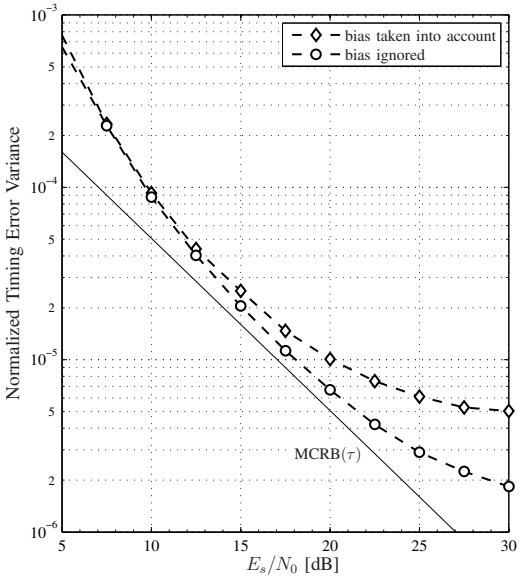

Fig. 3. MCRB vs. normalized timing error variance when the bias for TED-A is ignored and when it is taken into account. The modulation scheme is ARTM CPM ($M = 4$, 3RC, $h = \{4/16, 5/16\}$) with $BT_s = 1 \times 10^{-3}$.

Fig. 2 (b) shows analytical (data-aided) S-curves for TED-B in (29) for the 64-state 3×1 ARTM CPM detector. Unlike the curves for TED-A in Fig. 2 (a), TED-B does not exhibit a bias for different modulation index alignments; instead, there is only a slight variation in the slope and maximum amplitude of the curves. We point out that the final S-curves in Figs. 2 (a) and (b) (i.e. the curves with heavier line weights) are identical, which confirms the equivalence of (28) and (29).

The question of which TED formulation yields better tracking accuracy is addressed in Fig. 4. In this figure, we consider the 256-state, 48×2 MF optimal detector and the 64-state, 3×1 MF simplified detector, both with $BT_s = 1 \times 10^{-3}$. In the latter case, we include an additional scenario where $|\mathcal{K}_{\text{TED}}| = 2 \times 1$, where the smallest-amplitude MF/pulse is not used for the purposes of the TED. The best overall performance is obtained by TED-B using the optimal bank of $|\mathcal{K}_{\text{TED}}| = 48 \times 2$ MFs/pulses, which is a configuration that is exactly equivalent to one that would be obtained using a traditional (i.e. non-PAM) approach in [12]. The performance of all the reduced-complexity configurations is quite good for

[5]When the bias is taken into account, there is a timing offset in Fig. 1 between the MF sampling instants used for the VA and those used for the TED; this timing offset cycles with the modulation index alignment. When the bias is not taken into account, there is *no* timing offset between the VA and the TED.

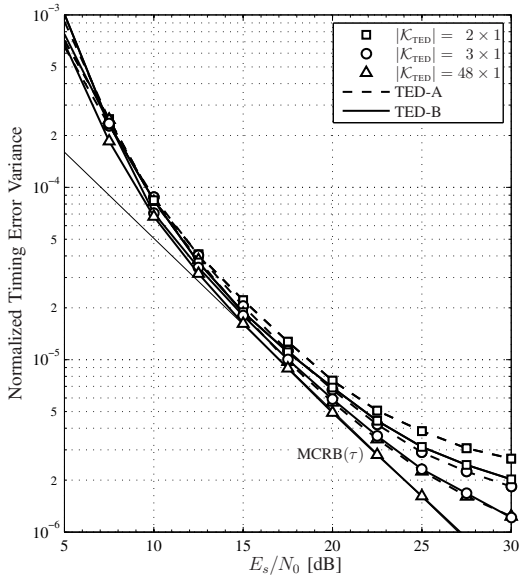

Fig. 4. MCRB vs. normalized timing error variance for various cases of ARTM CPM ($M = 4$, 3RC, $h = \{4/16, 5/16\}$) and $BT_s = 1 \times 10^{-3}$.

small values of E_s/N_0 but the TED-B configurations perform better for large values of E_s/N_0. In the examples considered next, the relative ranking between the two TED formulations often fluctuates depending on the operating range of E_s/N_0.

B. PCM/FM: $M = 2$, 2RC, $h = 7/10$

We next discuss the CPM scheme with $M = 2$, 2RC, and $h = 7/10$, which is known as "PCM/FM" (pulse code modulation/frequency modulation) in the IRIG 106-04 aeronautical telemetry standard [15]. The optimal PAM-based detector for this scheme requires a 20-state trellis and a bank of 2 MFs/pulses. We use a 10-state detector with $L' = 1$ that uses only $|\mathcal{K}| = |\mathcal{K}_{\text{TED}}| = 1$ MF/pulse, which is essentially optimum in terms of detection efficiency. The S-curves for this CPM scheme are shown in Fig. 5 for TED-A. S-curves for TED-B are not shown because there is no difference between the S-curves for the two TEDs.

Fig. 6 shows the normalized timing error variance results for the PCM/FM scheme, which are very close to the MCRB for most values of E_s/N_0. The most interesting finding for this CPM scheme is that the relative ranking between the two TEDs varies with E_s/N_0. TED-A is more effective than TED-B for smaller values of E_s/N_0. As E_s/N_0 increases, the normalized timing error variance of TED-A becomes worse than that of TED-B. However, this performance deviation occurs at values of E_s/N_0 that are too large to have any practical impact on the bit error rate (BER), which is a more important figure of merit than timing error variance in a digital communication system. In BER simulations (not shown here due to space constraints) over the range of E_s/N_0 shown in Fig. 6, there was no observable BER degradation for either TED at this loop bandwidth ($BT_s = 5 \times 10^{-3}$); however, some degradation would be expected for TED-B for small E_s/N_0 and wider loop bandwidths.

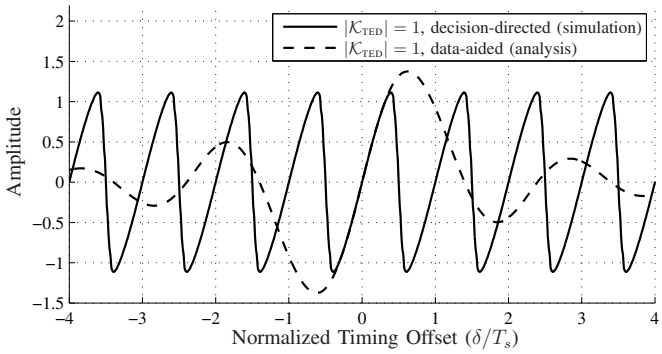

Fig. 5. Data-aided (analytical) and decision-directed (simulated) S-curves for PCM/FM ($M = 2$, 2RC, $h = 7/10$) with TED-A and $|\mathcal{K}_{\text{TED}}| = 1$. Curves are not shown for TED-B because they are identical to the ones shown here.

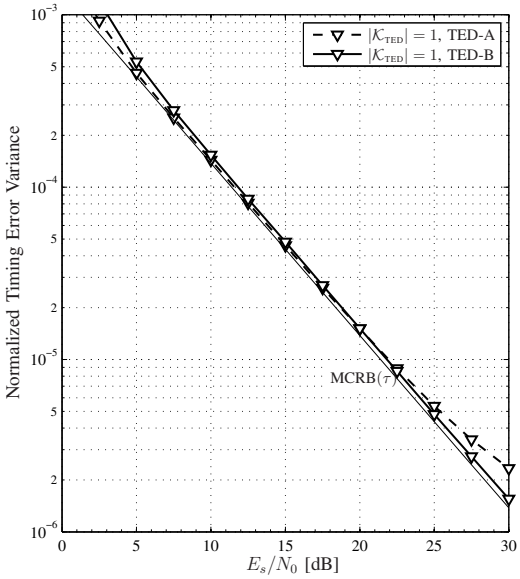

Fig. 6. MCRB vs. normalized timing error variance for various cases of PCM/FM ($M = 2$, 2RC, $h = 7/10$) and $BT_s = 5 \times 10^{-3}$.

C. SOQPSK-TG

Shaped-offset quatrature phase shift keying (SOQPSK) is a special type of CPM that uses a constrained ternary symbol alphabet. Background material on SOQPSK can be found in, e.g. [21], [22]. We consider the partial-response $L = 8$ version of SOQPSK used by the telemetry group, known as "SOQPSK-TG" in the IRIG 106-04 aeronautical telemetry standard [15]. The optimal PAM-based detector for this scheme requires a 512-state trellis and a bank of 4374 MFs/pulses [23]. We use a 4-state detector with $L' = 1$ that uses $|\mathcal{K}| = 2$ MFs/pulses, which is suboptimum by 0.1 dB in terms of detection efficiency [22]. Due to the extreme shortening of L', the decision feedback implementation for TED-B is not practical. The S-curves for TED-A for this CPM scheme are shown in Fig. 7 for $|\mathcal{K}_{\text{TED}}| = 2$ and $|\mathcal{K}_{\text{TED}}| = 1$; the main difference between these two cases is the amplitude of the S-curve, which is consistent with the large amplitude of the PAM pulse that is discarded in the $|\mathcal{K}_{\text{TED}}| = 1$ configuration

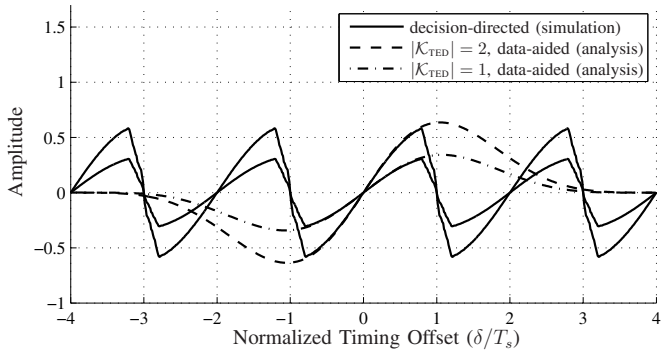

Fig. 7. Data-aided (analytical) and decision-directed (simulated) S-curves for SOQPSK-TG with TED-A, $|\mathcal{K}_{\text{TED}}| = 2$, and $|\mathcal{K}_{\text{TED}}| = 1$.

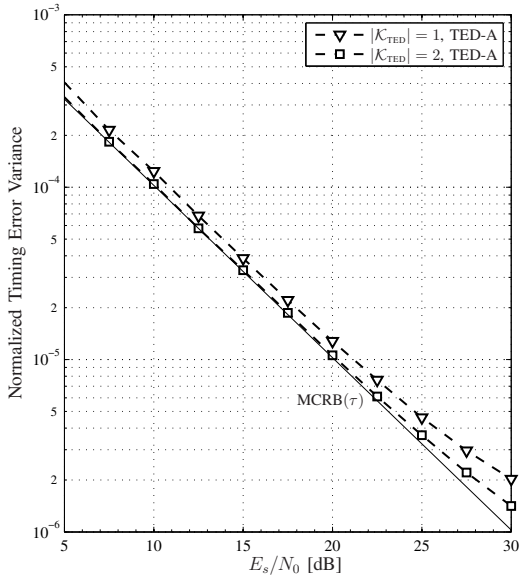

Fig. 8. MCRB vs. normalized timing error variance for various cases of SOQPSK-TG and $BT_s = 1 \times 10^{-3}$.

(see [22, Fig. 6]). Although SOQPSK-TG has $N_h = 1$ modulation index, there is an n-even/n-odd dependence in the SOQPSK signal model [21], [22] which gives rise to the period of $2T_s$ for the decision-directed S-curves in Fig. 7.

Fig. 8 shows the normalized timing error variance results for the two SOQPSK-TG configurations, where we see that the $|\mathcal{K}_{\text{TED}}| = 2$ configuration is very close to the MCRB except for larger values of E_s/N_0. The $|\mathcal{K}_{\text{TED}}| = 1$ case has the same basic shape but is inferior by around 1 dB.

VI. Conclusion

We have shown how the PAM representation of M-ary multi-h CPM can be applied to the problem of symbol timing recovery for CPMs in general. We have developed two slightly-different formulations of PAM-based TEDs, and have analyzed and compared their performance. The relative ranking between the two formulations fluctuates depending on the particular CPM scheme and the operating range of E_s/N_0. Therefore, there is no unanimous opinion in choosing between the two formulations. In general, both formulations have low complexity and are able to perform close to the MCRB. As such, the proposed TEDs provide an important synchronization component for reduced-complexity PAM-based CPM receivers that has been missing up to this point.

References

[1] J. B. Anderson, T. Aulin, and C.-E. Sundberg, *Digital Phase Modulation*. New York: Plenum Press, 1986.

[2] P. A. Laurent, "Exact and approximate construction of digital phase modulations by superposition of amplitude modulated pulses (AMP)," *IEEE Trans. Commun.*, vol. 34, pp. 150–160, Feb. 1986.

[3] U. Mengali and M. Morelli, "Decomposition of M-ary CPM signals into PAM waveforms," *IEEE Trans. Inform. Theory*, vol. 41, pp. 1265–1275, Sep. 1995.

[4] E. Perrins and M. Rice, "PAM decomposition of M-ary multi-h CPM," *IEEE Trans. Commun.*, vol. 53, pp. 2065–2075, Dec. 2005.

[5] X. Huang and Y. Li, "The PAM decomposition of CPM signals with integer modulation index," *IEEE Trans. Commun.*, vol. 51, pp. 543–546, Apr. 2003.

[6] M. P. Wylie-Green, "A new finite series expansion for continuous phase modulated waveform," *IEEE Trans. Commun.*, vol. 55, pp. 1547–1556, Aug. 2007.

[7] G. K. Kaleh, "Simple coherent receivers for partial response continuous phase modulation," *IEEE J. Sel. Areas Commun.*, vol. 7, pp. 1427–1436, Dec. 1989.

[8] G. Colavolpe and R. Raheli, "Reduced-complexity detection and phase synchronization of CPM signals," *IEEE Trans. Commun.*, vol. 45, pp. 1070–1079, Sep. 1997.

[9] E. Perrins and M. Rice, "A new performance bound for PAM-based CPM detectors," *IEEE Trans. Commun.*, vol. 53, pp. 1688–1696, Oct. 2005.

[10] A. N. D'Andrea, A. Ginesi, and U. Mengali, "Frequency detectors for CPM signals," *IEEE Trans. Commun.*, vol. 43, pp. 1828–1837, Feb./Mar./Apr. 1995.

[11] A. N. D'Andrea, U. Mengali, and M. Morelli, "Symbol timing estimation with CPM modulation," *IEEE Trans. Commun.*, vol. 44, pp. 1362–1372, Oct. 1996.

[12] M. Morelli, U. Mengali, and G. M. Vitetta, "Joint phase and timing recovery with CPM signals," *IEEE Trans. Commun.*, vol. 45, pp. 867–876, Jul. 1997.

[13] Q. Zhao and G. L. Stüber, "Robust time and phase synchronization for continuous phase modulation," *IEEE Trans. Commun.*, vol. 54, pp. 1857–1869, Oct. 2006.

[14] M. Morelli and G. M. Vitetta, "Joint phase and timing recovery for MSK-type signals," *IEEE Trans. Commun.*, vol. 48, pp. 1997–1999, Dec. 2000.

[15] Range Commanders Council Telemetry Group, Range Commanders Council, White Sands Missile Range, New Mexico, *IRIG Standard 106-04: Telemetry Standards*, 2004. (Available on-line at http://www.ntia.doc.gov/osmhome/106.pdf).

[16] J. Proakis and M. Salehi, *Digital Communications*. New York: McGraw-Hill, 2008.

[17] B. E. Rimoldi, "A decomposition approach to CPM," *IEEE Trans. Inform. Theory*, vol. 34, pp. 260–270, Mar. 1988.

[18] A. N. D'Andrea, U. Mengali, and R. Reggiannini, "The modified Cramer-Rao bound and its application to synchronization problems," *IEEE Trans. Commun.*, vol. 42, pp. 1391–1399, Feb./Mar./Apr. 1994.

[19] U. Mengali and A. N. D'Andrea, *Synchronization Techniques for Digital Receivers*. New York: Plenum Press, 1997.

[20] E. Perrins and M. Rice, "Reduced complexity detectors for multi-h CPM in aeronautical telemetry," *IEEE Trans. Aerosp. Electron. Syst.*, vol. 13, pp. 286–300, Jan. 2007.

[21] L. Li and M. Simon, "Performance of coded OQPSK and MIL-STD SOQPSK with iterative decoding," *IEEE Trans. Commun.*, vol. 52, pp. 1890–1900, Nov. 2004.

[22] E. Perrins and M. Rice, "Reduced-complexity approach to iterative detection of SOQPSK," *IEEE Trans. Commun.*, vol. 55, pp. 1354–1362, Jul. 2007.

[23] E. Perrins and M. Rice, "PAM representation of ternary CPM," to be published in *IEEE Trans. Commun.*